JACS
JOURNAL OF THE AMERICAN CHEMICAL SOCIETY
Article
pubs.acs.org/JACS

Variable Pathways for Oxygen Atom Insertion into Metal−Carbon Bonds: The Case of Cp*W(O)$_2$(CH$_2$SiMe$_3$)

Jiajun Mei,[†] Kurtis M. Carsch,[‡] Cody R. Freitag,[‡] T. Brent Gunnoe,*[,†] and Thomas R. Cundari*[,‡]

[†]Department of Chemistry, University of Virginia, Charlottesville, Virginia 22904-4319, United States

[‡]Department of Chemistry and Center for Advanced Scientific Computing and Modeling, University of North Texas, Denton, Texas 76203-5017, United States

Supporting Information

ABSTRACT: Cp*W(O)$_2$(CH$_2$SiMe$_3$) (**1**) (Cp* = η^5-pentamethylcyclopentadienyl) reacts with oxygen atom donors (e.g., H_2O_2, PhIO, IO_4^-) in THF/water to produce TMSCH$_2$OH (TMS = trimethylsilyl). For the reaction of **1** with IO_4^-, the proposed pathway for alcohol formation involves coordination of IO_4^- to **1** followed by concerted migration of the −CH$_2$TMS ligand to the coordinated oxygen of IO_4^- with concomitant dissociation of IO_3^- to produce Cp*W(O)$_2$(OCH$_2$SiMe$_3$) (**3**), which undergoes protonolysis to yield free alcohol. In contrast to the reaction with IO_4^-, the reaction of **1** with H_2O_2 results in the formation of the η^2-peroxo complex Cp*W(O)(η^2-O$_2$)(CH$_2$SiMe$_3$) (**2**). In the presence of acid (HCl) or base (NaOH), complex **2** produces TMSCH$_2$OH. The conversion of **2** to TMSCH$_2$OH catalyzed by Brønsted acid is proposed to occur through protonation of the η^2-peroxo ligand, which facilitates the transfer of the −CH$_2$TMS ligand to a coordinated oxygen of the η^2-hydroperoxo ligand. In contrast, the hydroxide promoted conversion of **2** to TMSCH$_2$OH is proposed to involve hydroxide coordination, followed by proton transfer from the hydroxide ligand to the peroxide ligand to yield a κ^1-hydroperoxide intermediate. The migration of the −CH$_2$TMS ligand to the coordinated oxygen of the κ^1-hydroperoxo produces an alkoxide complex, which undergoes protonolysis to yield free alcohol.

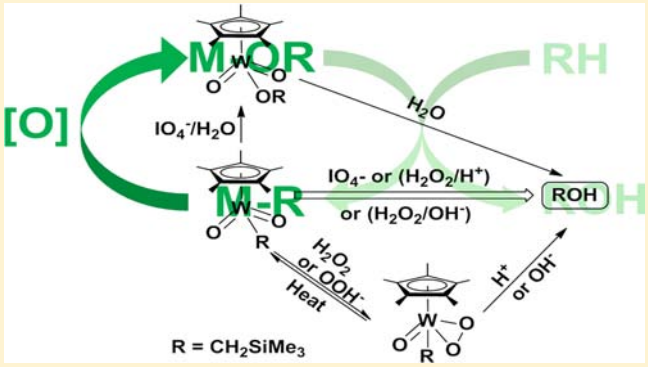

INTRODUCTION

Hydrocarbon oxidation is a fundamentally important process for the petrochemical industry.[1−3] The development of new catalysts for the selective oxidation of hydrocarbons, especially alkanes, has the potential to enhance the efficiency of production of chemicals and fuels.[4−11] However, the selective functionalization (e.g., direct partial oxidation) of alkanes is among the most challenging catalytic processes.

Transition-metal catalysts for the partial oxidation of alkanes to form alcohols must be able to perform two key steps: C−H bond activation and C−O bond formation. The Pt-based Shilov system, developed in the 1960s, was among the first homogeneous catalysts to successfully activate alkanes to form alcohols or alcohol precursors. It has been proposed that C−H bond activation occurs at Pt^{II} followed by C−X (X = OH or Cl) bond formation at Pt^{IV}−alkyl by reductive (i.e., reduction of Pt^{IV} to Pt^{II}) nucleophilic addition to an electrophilic Pt^{IV}−alkyl ligand.[12,13] The use of expensive Pt^{IV} as a stoichiometric oxidant to convert Pt^{II}−alkyl to Pt^{IV}−alkyl limits the utility of this catalyst.[12−14]

While C−X (X = OH or Cl) bond formation in the Shilov-type catalysts has been proposed to involve nucleophilic addition of water or halide to an electrophilic Pt^{IV}−alkyl ligand,[12] an alternative strategy for metal-mediated C−O bond formation involves net oxygen atom insertion into metal−alkyl bonds. For example, one possible catalytic cycle incorporates oxygen atom insertion into a M−R bond followed by C−H activation via net 1,2-addition across a M−OR bond to convert an alkane to an alcohol.[10,15−18] Scheme 1 shows two distinct pathways for oxygen atom insertion into M−R bonds from the

Scheme 1. Proposed Pathways for Partial Oxidation of Hydrocarbon Involving Oxygen Atom Insertion into a M−R Bond and 1,2-CH-Addition across a M−OR Bond

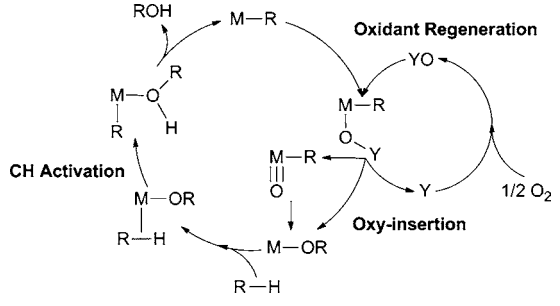

Received: October 2, 2012
Published: December 24, 2012

   dx.doi.org/10.1021/ja309755g | J. Am. Chem. Soc. 2013, 135, 424−435

reaction of a M−R moiety with an oxygen atom delivery reagent (YO). One pathway involves a migration of the ligand R to a metal-oxo intermediate. The second pathway incorporates direct oxy-insertion from M(OY)(R) without the formation of a metal-oxo intermediate. To be generally useful for selective oxidations at high conversion, ideally, the C−O bond forming step should proceed without the formation of radical intermediates and can be facilitated by catalysts including organocatalysts, as recently reported with flavinium-s,[19] and by metal-oxo complexes as reported by Goldberg and co-workers.[20]

The 1,2-addition of C−H bonds across M−NHR and M−OR bonds is known. In 2003, our groups studied and reported intramolecular C−H activation by a PCP−Ru^{II} amido complex and commented on the potential utility of this transformation in catalytic transformations.[21] Then, in 2005, we reported intermolecular benzene C−H activation by Ru^{II} hydroxide and anilide complexes.[17,22] Related chemistry includes an Ir^{III} complex and Ru^{II} complexes by Periana, Goddard, and co-workers,[16,23] a Rh^{I} complex reported by Heinekey, Goldberg, and co-workers,[24] and a Rh^{I} complex reported by Bercaw, Labinger, and co-workers.[25]

While insertions of oxygen atoms into M−C bonds are known, examples that occur by non-radical routes are rare. In a 1988 publication that focused on oxygen atom insertion into Ta^{V} hydrocarbyl bonds, Bercaw and co-workers stated, "The details of the actual oxygen-transfer step in controlled metal-mediated oxidations are still poorly understood...examples of clean carbon−oxygen bond formation for well-characterized compounds are rarer still."[26] Despite a few recent exam-ples,[15,19,27−31] we believe that this statement remains accurate.

Some early transition-metal complexes, such as group IV complexes, initiate oxygen atom insertion into M−R bonds; however, these reactions commonly proceed by radical pathways.[32,33] Brown and Mayer reported oxy-insertion into M−Ar (Ar = aryl) bonds with Re^{VII} via the migration of the Ar group to an oxo ligand.[29,31] Similar mechanisms that involve the formation of metal−oxo have also been proposed for the oxygen atom insertion of Pd complexes, but mechanistic studies have not been disclosed.[28,34] Hillhouse and co-workers have reported net oxygen insertion into a series of Ni−R bonds and a Hf−Ph bond upon reaction with N_2O.[30,35] Espenson and co-workers reported that methyltrioxorhenium (MTO) reacts with oxidants to release methanol.[36] Later, Periana, Goddard, and co-workers investigated the mechanism of this reaction. A pathway that involves migration of the methyl ligand to the oxygen of the coordinated oxidant was proposed, and an analogy between this reaction and the Baeyer−Villiger reaction (conversion of ketones to esters) was made.[15,37,38]

Given the importance of metal-mediated C−O bond formation, we have been interested in understanding mechanisms and strategies to facilitate these transformations. To our knowledge, detailed studies of reactions that give clean oxygen atom insertion into metal−hydrocarbyl bonds are limited to the studies of Re^{VII} complexes.[15,29,31,35,36] Herein, we present studies of oxygen atom insertion into the W−CH_2SiMe_3 bond of Cp*W(O)$_2$(CH_2SiMe_3) (**1**) and Cp*W(O)(η^2-O_2)(CH_2SiMe_3) (**2**). Complexes **1** and **2** have been previously prepared and studied by Legzdins and co-workers.[39]

RESULTS AND DISCUSSION

Reaction of Cp*W(O)$_2$(CH_2SiMe_3) (1) with $NaIO_4$. The reaction of Cp*W(O)$_2$(CH_2SiMe_3) (**1**) with H_2O_2 has been reported to yield the η^2-peroxo complex Cp*W(O)(η^2-O_2)(CH_2SiMe_3) (**2**);[39] however, the reaction of **1** with 1 equiv of $NaIO_4$ in 1:1 THF-d_8/D_2O or 1:1 1,4-dioxane-d_8/D_2O (v/v) does not produce complex **2**. Rather, $TMSCH_2OH$ (TMS = $SiMe_3$, trimethylsilyl) is formed without observation of **2** as an intermediate. The reaction is complete within two hours at room temperature and produces $TMSCH_2OH$ in almost 100% yield by ^{1}H NMR spectroscopy (eq 1). To determine the

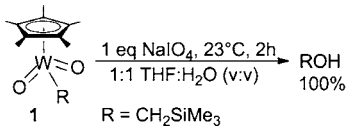

(1)

pathway for the conversion of **1** and $NaIO_4$ to $TMSCH_2OH$, we first considered the possibility that the η^2-peroxo complex Cp*W(O)(η^2-O_2)(CH_2SiMe_3) (**2**) is formed as an intermediate, followed by oxy-insertion into the W−C bond and subsequent protonolysis to give free $TMSCH_2OH$. Complex **2** was reacted with $NaIO_4$ under the same conditions as the alcohol release from **1** and $NaIO_4$, and no alcohol was observed by ^{1}H NMR spectroscopy after 24 hours. Furthermore, **2** does not react with $NaIO_3$ or D_2O to produce $TMSCH_2OH$ under the same conditions. Thus, the evidence suggests that the formation of $TMSCH_2OH$ from **1** and $NaIO_4$ does not likely proceed via complex **2**.

The reaction of **1** and $NaIO_4$ (5 equiv) in 1:1 THF-d_8/D_2O (v/v) was monitored at −1.3 °C by ^{1}H NMR spectroscopy. During the conversion, the disappearance of **1**, the emergence of an intermediate, and the appearance of $TMSCH_2OH$ were observed. The formation of $TMSCH_2OH$ occurs with $t_{1/2}$ ~40 min in approximately 100% yield. On the basis of ^{1}H NMR spectroscopy, the intermediate is proposed to be the tungsten alkoxide complex Cp*W(O)$_2$(OCH_2SiMe_3) (**3**); however, we were not able to isolate **3**. The ^{1}H NMR resonances of the intermediate **3** are assigned as 4.17 (CH_2, s), 2.04 (CH_3, s), −0.05 ($SiMe_3$, s) ppm. Mo(O)$_2$(OEt)$_2$ exhibits a resonance due to the OCH_2Me at 4.65 ppm,[40] and the similar complex (bpy)Mo(O)$_2$(OEt)$_2$ (bpy = 2,2′-bipyridine) exhibits a methylene resonance at 3.86 ppm.[41] In contrast, the CH_2 groups of **1** and **2** resonate at 0.43 and 3.16 ppm, respectively. In addition to $NaIO_4$, complex **1** reacts with iodosobenzene (PhI=O) in 1,4-dioxane at room temperature to produce **3** in ~20% yield in 20 min by ^{1}H NMR spectroscopy (eq 2); however, at prolonged reaction times, an intractable mixture of products is formed.

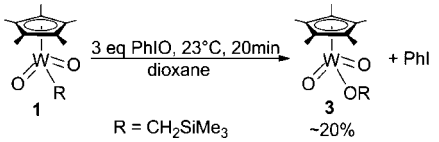

(2)

Figure 1 depicts the concentration versus time plot for all species observed in the conversion of **1** and $NaIO_4$ to $TMSCH_2OH$, based on the integrations of the methylene resonances of **1**, the $TMSCH_2OH$ product, and complex **3**. The sum of concentrations of these three species (black X's, Figure 1) remains constant over the course of the reaction.

Scheme 2 depicts a proposed organometallic Baeyer−Villiger (OMBV) pathway for the formation of $TMSCH_2OH$ from the reaction of **1** with $NaIO_4$. Periodate coordinates to complex **1**, followed by concerted migration of the alkyl ligand to the

dx.doi.org/10.1021/ja309755g | J. Am. Chem. Soc. 2013, 135, 424−435

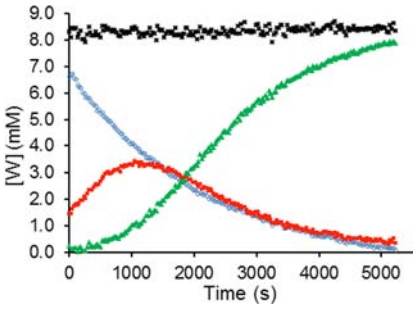

Figure 1. Plot of concentration versus time during the conversion of $Cp^*W(O)_2(CH_2SiMe_3)$ (**1**) and $NaIO_4$ (5 equiv) to $TMSCH_2OH$ (−1.3 °C in 1:1 THF-d_8/D_2O (v/v)) including complex **1** (blue, circles), $Cp^*W(O)_2(OCH_2SiMe_3)$ (**3**) (red, squares), $TMSCH_2OH$ (green, triangles), and the sum of all three species (black, X's).

Scheme 2. Proposed Mechanism for the Formation of $TMSCH_2OH$ from the Reaction of $Cp^*W(O)_2(CH_2SiMe_3)$ (1) and $NaIO_4$ in 1:1 THF-d_8/D_2O (v/v)

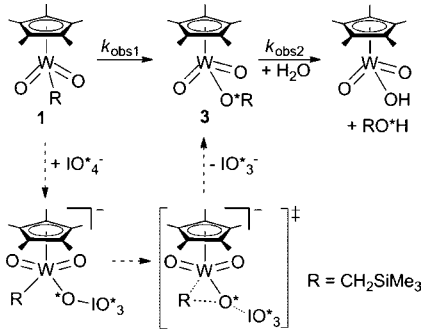

coordinated oxygen atom of IO_4^- and loss of IO_3^-. Protonation of complex **3** generates the alcohol product. Assuming that the oxygen atoms of coordinated IO_4^- do not exchange with the oxo ligands of the putative adduct $[Cp^*W(O)_2(OIO_3)(R)]^-$ in the proposed pathway, the oxygen atom in the $TMSCH_2OH$ product should be derived from the oxygen donor (i.e., IO_4^-) and not from complex **1**. Consistent with this hypothesis, gas chromatography/mass spectrometry (GC/MS) analysis of the reaction of $Cp^*W(^{16}O)_2(CH_2SiMe_3)$ with $NaI^{18}O_4$ shows that only $TMSCH_2{}^{18}OH$ is formed.

Using kinetic simulation (Kinetica98 software;[42] see the Supporting Information and the Experimental Section), rate constants for the formation of **3** (k_{obs1} = 8.46(1) × 10^{-4} s^{-1}) and the conversion of **3** to $TMSCH_2OH$ (k_{obs2} = 1.01(1) × 10^{-3} s^{-1}) were determined. In addition, under pseudo first-order conditions (i.e., excess IO_4^-), complex **1** was treated with a series of concentrations of $NaIO_4$ in 1:1 THF-d_8/D_2O (v/v) at −1.3 °C, and a rate constant k_{obs1} for the disappearance of complex **1** was determined for each reaction. A plot of k_{obs1} as a function of $[IO_4^-]$ shows a first-order dependence on $[IO_4^-]$ (Figure 2). Thus, the experimentally derived rate law for the conversion of **1** and IO_4^- to **3** is rate = $k_1[\mathbf{1}][IO_4^-]$, and the slope of the plot in Figure 2 gives k_1 = 1.9(3) × 10^{-2} $M^{-1}\cdot s^{-1}$ that corresponds to a $\Delta G^{\ddagger}$ = 18.0(1) kcal·mol^{-1} at −1.3 °C.

The conversion of **1** and $NaIO_4$ to **3** was monitored by ^1H NMR spectroscopy at −1.3, 10.7, 22.7, and 34.7 °C. An Eyring plot using k_1 (determined from the rate of disappearance of **1** divided by the $[IO_4^-]$; (Figure 3) was used to calculate $\Delta H^{\ddagger}$ = 8.5(2) kcal·mol^{-1} and $\Delta S^{\ddagger}$ = −35.2(7) cal·$mol^{-1}\cdot K^{-1}$ for the conversion of **1** to **3**. The relatively large $|\Delta S^{\ddagger}|$ for a bimolecular

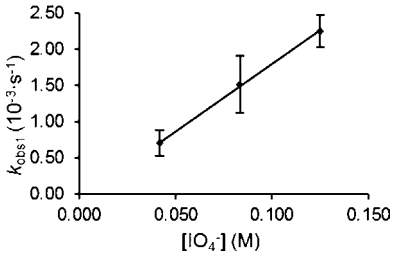

Figure 2. Plot of k_{obs1} vs $[IO_4^-]$ for the reaction of $Cp^*W(O)_2(CH_2SiMe_3)$ (**1**) with $NaIO_4$ showing a first-order dependence on $[IO_4^-]$ (R^2 = 0.99).

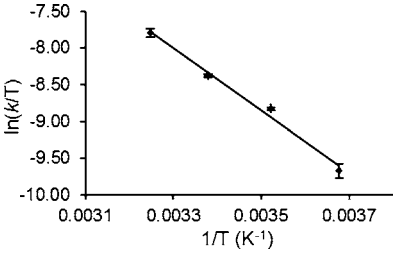

Figure 3. Plot of ln(k/T) vs 1/T for the conversion of $Cp^*W(O)_2(CH_2SiMe_3)$ (**1**) and $NaIO_4$ (5 equiv) to $Cp^*W(O)_2(OCH_2SiMe_3)$ (**3**) (R^2 = 0.99).

reaction indicates the possibility of substantial solvent ordering in the transition state.

Density functional theory (DFT) calculations were carried out to probe the mechanism for the reaction of **1** with IO_4^- to form $TMSCH_2OH$. Scheme 3 shows the energetics for the lowest energy pathway for **1** + IO_4^- → ROH that was calculated. The calculated free energy in 1,4-dioxane and water (1,4-dioxane/water) are given in Scheme 3. In the following text, we use the calculated numbers in 1,4-dioxane.

Through a combination of entropy and solvation effects (free IO_4^- is more heavily solvated than when coordinated to **1**), the

Scheme 3. Calculated Mechanism for the Release of $TMSCH_2OH$ in the Reaction of $Cp^*W(O)_2(CH_2SiMe_3)$ (1) with Periodate[a]

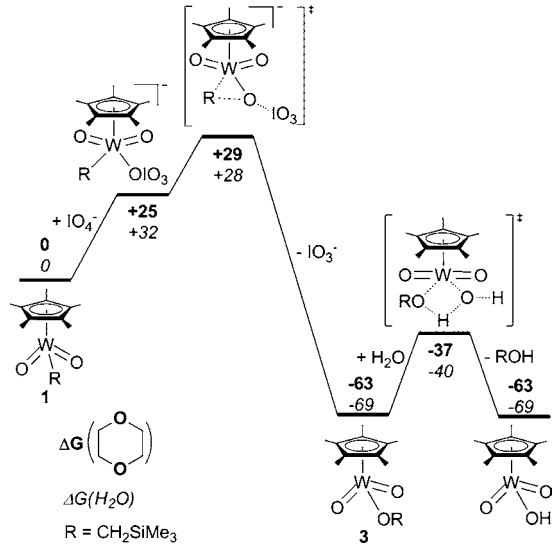

[a]Numbers are free energies (kcal·mol^{-1}) for 1,4-dioxane (top, bold) and water (bottom, italics) and are relative to complex **1** and IO_4^-.

dx.doi.org/10.1021/ja309755g | J. Am. Chem. Soc. 2013, 135, 424−435

formation of the adduct **1**−OIO_3^- is computed to be endergonic by ≥25 kcal·mol^{-1} in both solvents relative to separated **1** and periodate. Presumably, the inclusion of counterion effects would reduce the endergonicity of the reaction to form an anionic adduct and thus also the corresponding overall activation barrier of the formation of complex **3**. Periodate has been implicated in electron transfer reactions as well as two-electron oxygen atom transfer (OAT) chemistry.[43] To model the possibility of one-electron chemistry, we investigated the thermodynamics of the following electron transfer reaction: **1** + $[IO_4]^-$ → $\mathbf{1}^{\bullet-}$ + $[IO_4]^{\bullet}$. This reaction is decidedly endergonic in 1,4-dioxane (ΔG_{calc} = +120 kcal·mol^{-1}) and water (ΔG_{calc} = +122 kcal·mol^{-1}). In the absence of corroborating experimental data, quantitative significance should not be ascribed to the computed electron transfer thermodynamics. However, the significant computed endergonicity suggests that, for these Cp*W^{VI} complexes, the periodate anion is not likely acting as a single electron transfer reagent.

The DFT calculations support the hypotheses that oxygen atom insertion into the W−CH_2TMS bond upon reacting with IO_4^- occurs by an OMBV pathway. The calculated energy barrier for oxy-insertion from **1**−OIO_3^- is 28 kcal·mol^{-1} (PCM water). Part of the difference between the computed and experimental barriers is, as delineated below, due to the neglect of explicit solvation of the periodate oxidant and particularly its iodate leaving group. Multiple attempts (see the Supporting Information) to isolate alternative transition states (TSs) (e.g., a TS for formation of a peroxo leading to **2**, a [3 + 2] addition of periodate, etc.) either led to already found stationary points or the OMBV TS depicted in Figure 4 (the TS is modified

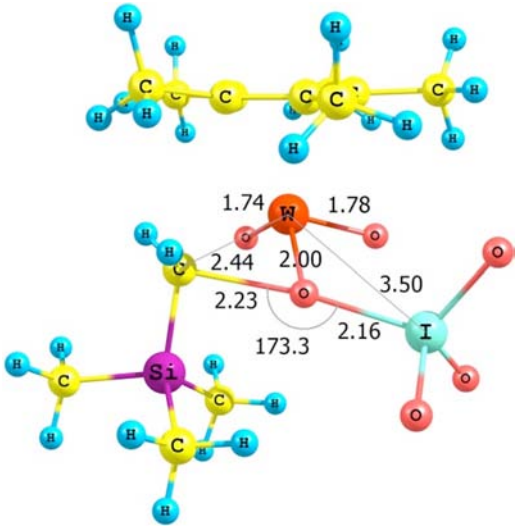

Figure 4. DFT-calculated TS for the oxy-insertion step of the overall reaction Cp*W(O)$_2$(CH_2SiMe_3) (**1**) + IO_4^- → Cp*W(O)$_2$(OCH_2SiMe_3) (**3**) + IO_3^-. Bond lengths are given in Å and bond angles in degrees.

based on studies of the impact of water, see below). The formation of **3** is calculated to be favorable, which is consistent with the observation of putative **3** as an intermediate in the overall reaction. The calculated I−O bond distance in the TS for oxygen atom insertion is 2.16 Å, which is much shorter than the 2.399 Å reported for the corresponding TS for MTO, implying an earlier TS for the Cp*W complex. The latter assertion is also supported by the calculated C−O distances for the carbon−oxygen bond being formed in the Baeyer−Villiger TS: 2.23 Å (for Cp*W complex) compared to 2.067 Å (MTO) TS.[15]

The reaction of complex **1** with $[Bu_4N][IO_4]$ (Bu = *n*-butyl) (3 equiv) in rigorously dried THF-d_8 results in no reaction even upon heating at 80 °C for 24 h, while the same starting material produced the intermediate **3** and ultimately $TMSCH_2OH$ in 1:1 THF-d_8/D_2O (v/v) at room temperature in hours. The failure of **1** and IO_4^- to produce free alcohol in the absence of water is perhaps not surprising, since the conversion of **3** to free alcohol requires a proton source. However, the lack of formation of **3** for the reaction of **1** and IO_4^- in the absence of water is less readily rationalized, especially since calculations show that the formation of **3** is favorable from **1** and IO_4^-. Water apparently facilitates the oxy-insertion reaction. Possible roles for water in the conversion of **1** and IO_4^- to **3** include the following: (1) as a solvent, water helps the ionization of the IO_4^- anion for metal coordination. (2) As an electron donor, water can coordinate the metal center resulting in a more electron-rich metal center and more nucleophilic −CH_2TMS ligand, which is analogous to the role of pyridine in the conversion of MTO and pyridine-*N*-oxide to the oxy-insertion product.[15,44] (3) Water interacts with coordinated IO_4^- to facilitate the dissociation of IO_3^-.

Under pseudo first-order conditions, the reaction of **1** and excess $[Bu_4N][IO_4]$ (15 equiv) with various amounts of D_2O in THF-d_8 was monitored at 50 °C by ^{1}H NMR spectroscopy. Kinetic plots reveal a first-order decay of **1**, and a plot of k_{obs} (divided by the $[IO_4^-]$) as a function of $[D_2O]$ shows that the decay of **1** with $[Bu_4N][IO_4]$ has a second-order dependence on $[D_2O]$ (Figure 5). Thus, the overall rate law for the

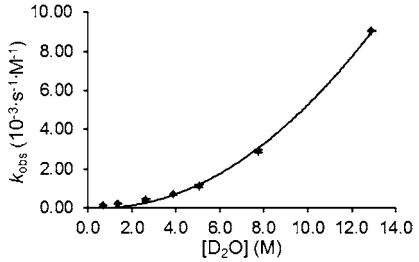

Figure 5. Plot of k_{obs} vs $[D_2O]$ for the reaction of Cp*W(O)$_2$(CH_2SiMe_3) (**1**) and excess $[Bu_4N][IO_4]$ (15 equiv) in THF-d_8 with various amounts of D_2O showing a second-order dependence on $[D_2O]$ (R^2 = 0.99).

conversion of **1** and IO_4^- to $TMSCH_2OH$ is rate = $k[\mathbf{1}][IO_4^-][D_2O]^2$. A fit of the plot in Figure 5 gives k = 5.8(2) × 10^{-5} M^{-3}·s^{-1} after dividing by $[IO_4^-]$ that corresponds to a $\Delta G^{\ddagger}$ = 25.2(1) kcal·mol^{-1} at 50 °C. The participation of water in the reaction is consistent with the relatively large $|\Delta S^{\ddagger}|$.

The role of water in the reaction of **1** and periodate was investigated computationally. Attempts to model a four-legged piano stool complex with inner-coordination sphere water, Cp*W(O)$_2$(OH_2)R, led instead to an outer-coordination sphere aqua complex in which water is hydrogen bonded to an oxo ligand. The possibility that water enhances the oxidizing potential of IO_4^- was probed computationally in several ways. The calculation of the OAT free energy for IO_4^- → IO_3^- + $^1/_2O_2$ is exergonic by −17 kcal·mol^{-1} in the gas phase.

dx.doi.org/10.1021/ja309755g | J. Am. Chem. Soc. 2013, 135, 424−435

Inclusion of continuum solvent effects (CPCM, water solvent) increases the exergonicity of this reaction to −26 kcal·mol^{-1}. The calculations indicate that the increased driving force results from more favorable solvation of the smaller iodate ion in relation to periodate. Thus, the calculations predict that water should enhance the thermodynamics of oxygen atom transfer from IO_4^-, but the extent to which this would enhance the oxy-insertion kinetics is uncertain without calculation of the corresponding hydrated OMBV transition state.

Explicit solvation effects on periodate-mediated OMBV reactions were modeled. Hydrogen bonding a water molecule to each oxo of the iodate leaving group in the OMBV TS results in a reduction of the calculated energy barrier from 28 kcal·mol^{-1} (Scheme 3) to 24 kcal·mol^{-1} (Figure 6), which is

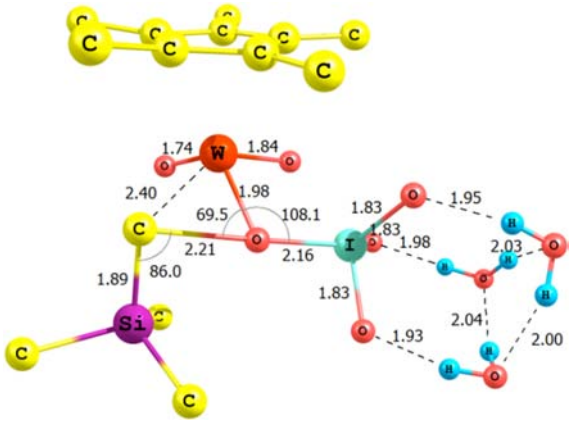

Figure 6. DFT-calculated TS with water for the oxy-insertion step of the overall reaction Cp*W(O)$_2$(CH$_2$SiMe$_3$) (**1**) + IO_4^- → Cp*W(O)$_2$(OCH$_2$SiMe$_3$) (**3**) + IO_3^-. Bond lengths are given in Å and bond angles in degrees.

closer to the experimental value of 18 kcal·mol^{-1} (see above). Bond lengths within the active site of the OMBV TS (Figure 4) are little changed upon hydrogen bonding with three water molecules. What is more noticeable is the shortening of the O−H−O hydrogen bonds by 0.05 Å from 2.00 Å ($[IO_4(OH_2)_3]^-$) to 1.95 Å in the oxy-insertion TS. In conjunction with the implicit solvation results above, these data lend credence to the proposal that preferential solvation of the iodate leaving group enhances oxy-insertion of periodate into the W−C bond of **1** both kinetically and thermodynamically, effectively making the iodate a better leaving group and the periodate a more potent oxidant.

Reaction of Cp*W(O)(η^2-O$_2$)(CH$_2$SiMe$_3$) with NaOH. Complex **2** reacts with NaOH to produce TMSCH$_2$OH in 1:1 THF-d_8/D$_2$O or 1,4-dioxane-d_8/D$_2$O (v/v). The reaction produces TMSCH$_2$OH in quantitative yield (^{1}H NMR) after 3 h at room temperature (eq 3).

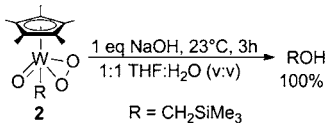

(3)

Under pseudo first-order conditions, the reaction of **2** with NaOH in 1:1 THF-d_8/D$_2$O (v/v) was monitored at 10.7 °C by ^{1}H NMR spectroscopy. Kinetic plots reveal a first-order decay of **2**, and a plot of k_{obs} as a function of [OH$^-$] shows that the reaction of **2** with NaOH has a first-order dependence on [OH$^-$] (Figure 7). The slope of the plot in Figure 7 gives k = 1.30(6) × 10^{-2} M^{-1}·s^{-1}, which corresponds to $\Delta G^{\ddagger}$ = 19.1(1) kcal·mol^{-1} at 10.7 °C.

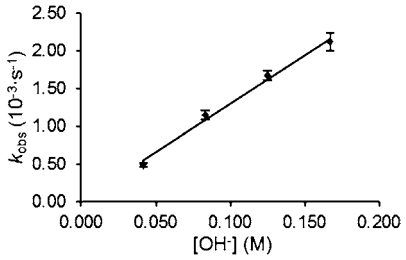

Figure 7. Plot of k_{obs} vs [OH$^-$] for the reaction of Cp*W(O)(η^2-O)$_2$(CH$_2$SiMe$_3$) (**2**) with NaOH showing a first-order dependence on [OH$^-$] (R^2 = 0.99).

The rate of the reaction between **2** and NaOH was monitored by ^{1}H NMR spectroscopy at −1.3, 10.7, 22.7, and 34.7 °C. An Eyring plot (using k values that were corrected for [HO$^-$], Figure 8) was used to calculate $\Delta H^{\ddagger}$ = 13.6(4) kcal·mol^{-1} and $\Delta S^{\ddagger}$ = −20(1) cal·mol^{-1}·K^{-1}.

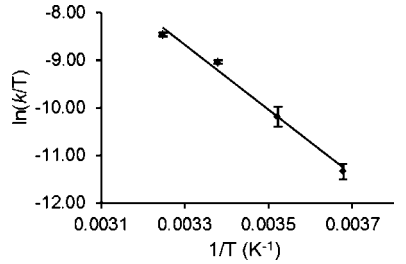

Figure 8. Plot of ln(k/T) vs 1/T for the reaction of Cp*W(O)(η^2-O)$_2$(CH$_2$SiMe$_3$) (**2**) with NaOH (5 equiv) (R^2 = 0.99).

Three possible pathways for the reaction of complex **2** with NaOH are shown in Scheme 4. In pathway A, the hydroxide undergoes direct nucleophilic addition to the TMSCH$_2$ ligand. For this pathway, the oxygen atom in the alcohol would

Scheme 4. Possible Pathways for Alcohol Release from the Reaction of Cp*W(O)(η^2-O)$_2$(CH$_2$SiMe$_3$) (2) with NaOH in 1:1 THF-d_8/D$_2$O (v/v)

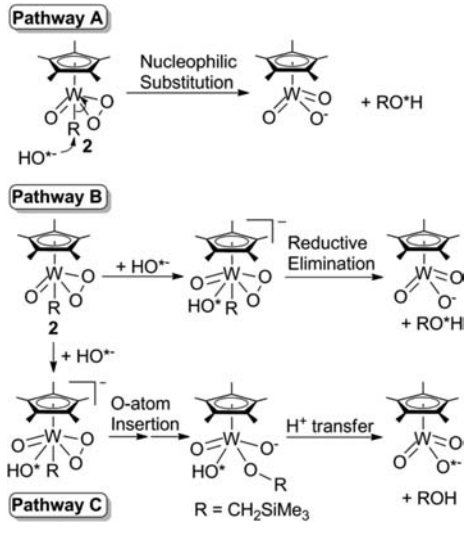

dx.doi.org/10.1021/ja309755g | J. Am. Chem. Soc. 2013, 135, 424−435

Scheme 5. Calculated Free Energy for the Reaction of Cp*WO(η^2-O)$_2$(CH_2SiMe_3) (2) with OH^-[a]

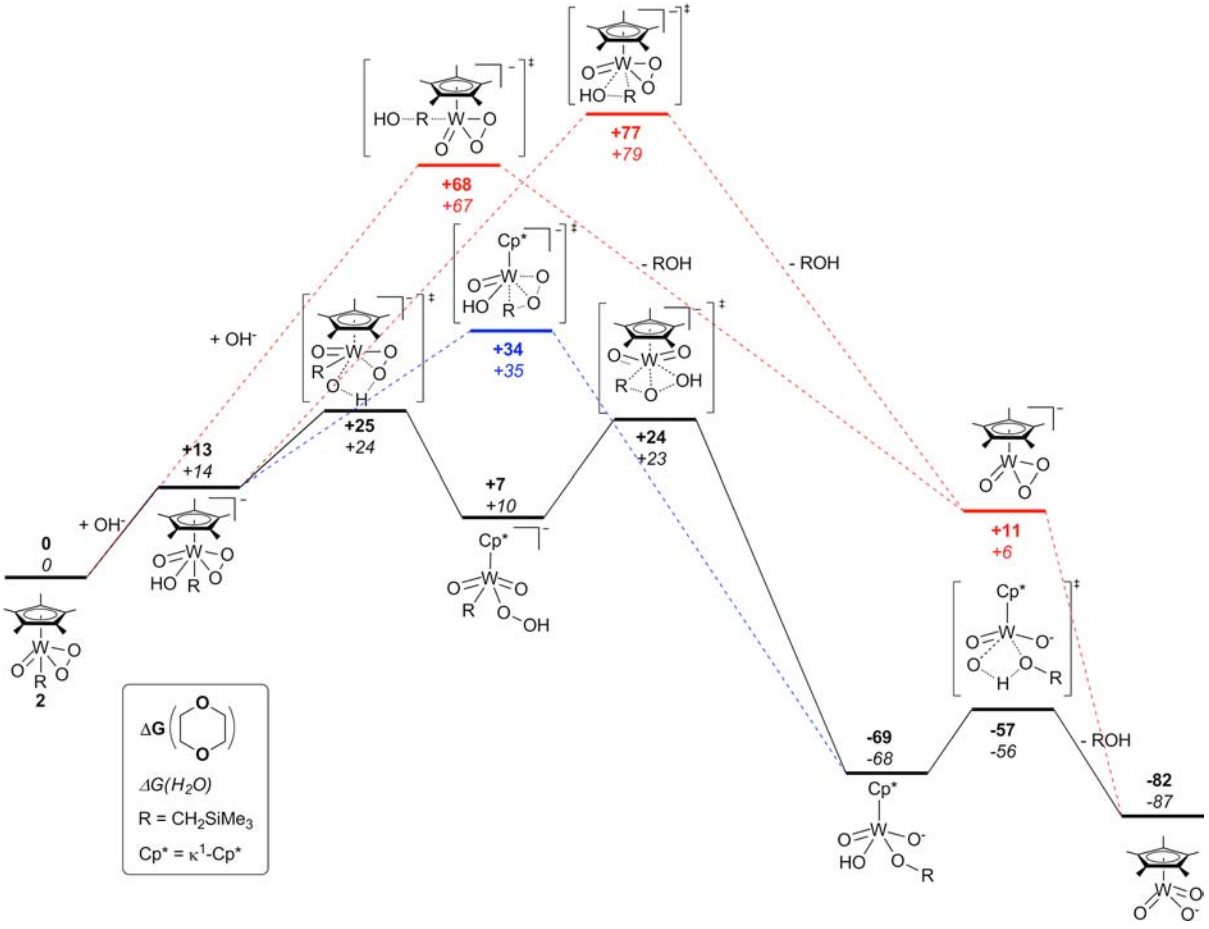

[a]Numbers are free energies (kcal·mol^{-1}) for 1,4-dioxane (top, bold) and water (bottom, italics) and are relative to complex **2** (Cp* = κ^1-Cp*).

originate from hydroxide. Pathway B involves hydroxide coordination to W followed by C−O reductive elimination. In pathway B, the oxygen atom of the alcohol would also originate from hydroxide. Pathway C involves hydroxide coordination to W, which would facilitate transfer of the $-CH_2TMS$ ligand to an η^2-peroxo oxygen atom. Protonation with water generates alcohol. The oxygen atom of the alcohol in pathway C originates from complex **2**. MeLi was reacted with ^{18}O-labeled water to generate the ^{18}O-labeled Li^{18}OH in $H_2{}^{18}O$. The alcohol product from the reaction of **2** with Li^{18}OH was then analyzed by GC/MS. Only R^{16}OH was observed in the MS spectrum, which is consistent with pathway C and inconsistent with pathways A and B in Scheme 4.

The role of hydroxide for the conversion of **2** to $TMSCH_2OH$ was probed computationally. Several mechanisms were investigated (Scheme 5). The very large calculated free energy barriers (≥67 kcal·mol^{-1}) led us to discount nucleophilic substitution (pathway A) and reductive elimination (pathway B). The calculations suggest that the hydroxide coordination-assisted alkyl migration to an oxygen atom of the η^2-peroxo ligand (34 and 35 kcal·mol^{-1} in 1,4-dioxane and water) has almost the same energy barrier as the non-assisted alkyl migration (35 and 32 kcal·mol^{-1} in 1,4-dioxane and water) (see Scheme 7 below). What emerged as the most reasonable pathway was a H atom transfer pathway in which hydroxide coordinates to **1**, followed by proton transfer ($\Delta G^{\ddagger}$ = 25 and 24 kcal·mol^{-1} in 1,4-dioxane and water, respectively) to yield a hydroperoxide intermediate, [(κ^1-Cp*)W(O)$_2$(R)(OOH)]$^-$ (Scheme 5). The OMBV TS from the latter is calculated to be 24 and 23 kcal·mol^{-1} in 1,4-dioxane and water above the starting complex **1**, in reasonable agreement with the experimental measurement. After oxy-insertion, hydroxide loss (to yield **3** + OH^-) or proton transfer (to yield [Cp*W(O)$_3$]$^-$ + ROH) was determined to be facile ($\Delta G^{\ddagger}$ = 12 kcal·mol^{-1} in 1,4-dioxane and water, respectively).

Scheme 6. Two Possible Pathways for the Alcohol Release Reaction of Cp*WO(η^2-O)$_2$(CH_2SiMe_3) (2) with HCl

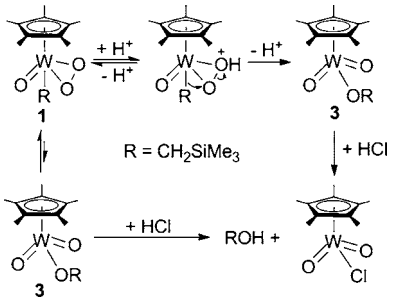

The calculated transition state for oxy-insertion from [(κ^1-Cp*)W(O)$_2$(R)(OOH)]$^-$ (Figure 9) is structurally similar to the corresponding TS for the transition state involving oxygen atom insertion from periodate (Figure 4). The C−O bond being formed is longer (2.23 vs 2.10 Å) and the W−C bond

dx.doi.org/10.1021/ja309755g | J. Am. Chem. Soc. 2013, 135, 424−435

Scheme 7. Calculated Free Energy for the Reaction of $Cp^*WO(\eta^2\text{-}O)_2(CH_2SiMe_3)$ (2) with H^+[a]

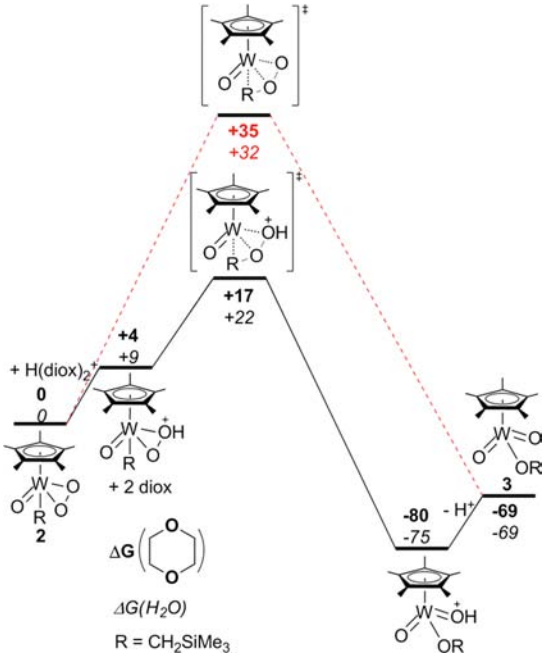

[a]The cation $(H(diox)_2^+$ (diox =1,4-dioxane)) was used to model the proton. Numbers are free energies (kcal·mol^{-1}) for 1,4-dioxane (top, bold) and water (bottom, italics) and are relative to complex **2**.

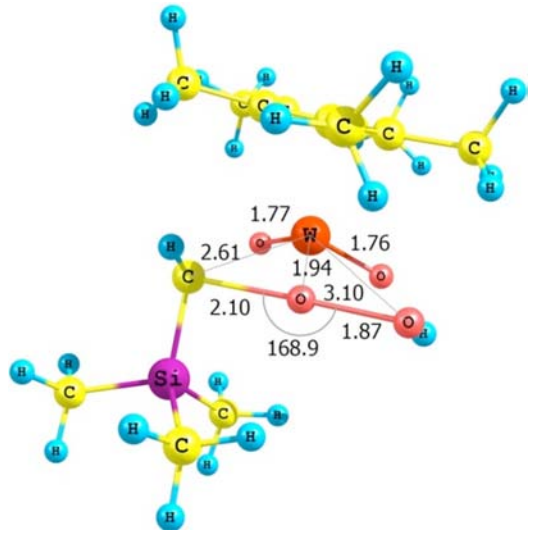

Figure 9. DFT calculated organometallic Baeyer–Villiger (OMBV) transition state for oxy-insertion of hydroperoxide into W–C bond of $Cp^*W(O)_2(CH_2SiMe_3)$ (**1**). Bond lengths are given in Å and bond angles in degrees.

being broken is shorter (2.44 vs 2.61 Å) for the periodate TS, implying an earlier TS for the OMBV oxy-insertion with periodate in relation to the hydroperoxide congener. The tremendous kinetic and thermodynamic free energy preference for the OMBV pathway in relation to the pathways that lead to reduced W^{IV} intermediates (nucleophilic substitution and reductive elimination, Scheme 5) is interesting in connection with the highly endergonic single-electron transfer reaction modeled above, and supports the notion of the important role of metal d orbital occupation in oxy-insertion, and further that movement away from d^0 motifs will disfavor the OMBV pathway. Thus, while functionalization of alkyl ligands through processes that formally reduce the metal center can be facile for late transition metal complexes, similar reactions with middle transition metals may have inherently and prohibitively high activation barriers.

Reaction of $Cp^*W(O)(\eta^2\text{-}O_2)(CH_2SiMe_3)$ (2) with Brønsted Acid. The formation of alcohol is also observed when complex **2** is treated with HCl in 1,4-dioxane. The reaction is complete in 40 h at room temperature and produces $Cp^*W(O)_2Cl$ and $TMSCH_2OH$ in ∼90% yield by ^1H NMR spectroscopy (eq 4). The acid-promoted reaction of **2** is slower

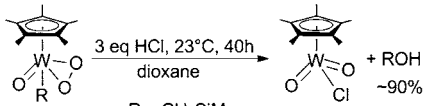

(4)

than the hydroxide-promoted conversion. For example, complex **2** with 3 equiv of NaOH quantitatively forms $TMSCH_2OH$ in less than 1 h at room temperature.

Table 1 shows the conditions and results for the reactions of complex **2** with various proton sources. Without a proton source, when **2** is heated in benzene at 80 °C for 24 h, no alcohol is observed, and the starting material decomposes to form complex **1** (entry 1). Heating increases the rate of conversion but decreases the yield (entries 3 and 4). The use of strong acid in 1,4-dioxane results in decomposition of the starting material with no alcohol production (entries 7 and 9). Adding $[^nBu_4N][Cl]$ does not accelerate the reaction, which is consistent with the acceleration by HCl resulting from the addition of protons rather than chloride. Also, weaker acids, such as lutidinium, do not facilitate this reaction at room temperature.

Table 1. Reaction Conditions and Yields for Reaction of $Cp^*W(O)(\eta^2\text{-}O)_2(CH_2SiMe_3)$ (2) with Brønsted Acid

no.	solvent	acid	T (°C)	t (h)	yield[a] (%)
1	benzene	none	80	24	0
2	dioxane[b]	3 equiv of HCl (Et_2O)	23	40	∼90
3	dioxane	3 equiv of HCl (dioxane)	23	32	∼70
4	dioxane	3 eq HCl (dioxane)	50	2	∼60
5	dioxane/water	3 equiv of HCl (35%)	23	100	∼80
6	dioxane/water	5 equiv of H_2SO_4 (98%)	23	100	>90
7	dioxane	5 equiv of H_2SO_4 (98%)	23	12	decomp.
8	dioxane/water	none	75	24	∼70
9	dioxane	HOTf (99%)	23	12	decomp.

[a]Yields of $TMSCH_2OH$ are based on integration of ^1H NMR spectra versus an internal standard. [b]1,4-dioxane.

We have considered two roles for the acid in the conversion of **2** and HCl to $Cp^*W(O)_2Cl$ and $TMSCH_2OH$ (Scheme 6): (1) the proton serves as a catalyst by protonating the η^2-peroxo ligand, which would increase oxygen electrophilicity and facilitate oxy-insertion. A similar mechanism was proposed for the acid-catalyzed rearrangement of an η^2-peroxo Ta alkyl to form oxo-alkoxide derivatives.[26] (2) The proton is not a catalyst, but rather, the acid serves to generate free alcohol from $Cp^*W(O)_2(OCH_2SiMe_3)$.

To investigate rate dependence of the reaction of **2** and HCl, we attempted to use excess HCl to achieve pseudo first-order

dx.doi.org/10.1021/ja309755g | J. Am. Chem. Soc. 2013, 135, 424–435

conditions. However, when more than 5 equiv of HCl are used, complex **2** decomposed with little production of $TMSCH_2OH$.

Reaction coordinates for conversion of **1** to **3** in the absence and presence of a proton were evaluated computationally to help assess the impact of Brønsted acids upon the proposed mechanisms of oxy-insertion. Various basic sites were evaluated in the starting materials, products, intermediates, and transition sites (e.g., protonation of oxo versus peroxo ligands). The discussion focuses on the most stable tautomers (Scheme 7). In the absence of a proton, the migration of R to the peroxide moiety has a calculated activation barrier of 35 or 32 kcal·mol^{-1} in 1,4-dioxane or water, respectively. Upon protonation (the protonated bis-dioxane cation, $[(dioxane)_2H]^+$, was used to model HCl in dioxane), the corresponding barriers were reduced to 17 kcal·mol^{-1} (1,4-dioxane) or 22 kcal·mol^{-1} (water). The results thus support the observation of acceleration of the oxy-insertion reaction upon the introduction of Brønsted acids.

Analysis of the calculated oxy-insertion TS geometries from **2** with and without an added proton is revealing (Figure 10). The

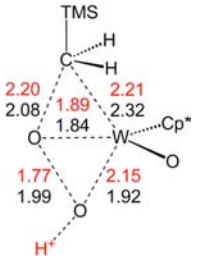

Figure 10. Calculated TS for oxy-insertion of Cp*W(O)(η^2-O)$_2$(CH_2SiMe_3) (**2**) with (red) and without (black) an added proton. Bond lengths are given in Å.

various bond distances in the active site point to an earlier TS upon the introduction of a proton, which is consistent with a lower barrier according to the Hammond postulate. Additionally, one may hypothesize that the protonation of the incipient oxide group in the peroxo TS yields a better leaving group (hydroxide). The greater exergonicity for neutral Cp*W(O)(η^2-O)$_2$R → Cp*W(O)$_2$(OR) versus the protonated variant (−69 kcal·mol^{-1} in 1,4-dioxane (Scheme 5) versus −80 kcal·mol^{-1} (Scheme 7)) provides additional support for these proposals and the role of Brønsted acids in catalyzing oxy-insertion from **2**.

Reaction of Cp*W(O)$_2$(CH_2SiMe_3) (1) with Hydrogen Peroxide in the Presence of Hydroxide. The reaction of complex **1** with H_2O_2 (3 equiv) in benzene generates complex **2** at room temperature after 24 h without production of alcohol. However, alcohol production is observed at room temperature when complex **1** is treated with a mixture of H_2O_2 (3 equiv) with NaOH (3 equiv) in 1:1 THF-d_8/D_2O (v/v). The reaction is complete in ∼4 h and produces $TMSCH_2OH$ in >95% yield by ^{1}H NMR spectroscopy (eq 5).

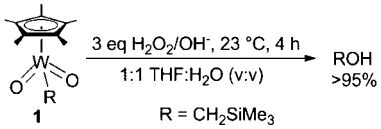

(5)

Espenson and co-workers observed faster decomposition and methanol release from MTO with H_2O_2 in a basic environment;[36] Periana, Goddard, and co-workers studied the mechanism for the reaction of MTO with H_2O_2 in the presence of hydroxide.[37] Calculations show that the OMBV pathway in which OOH^- coordinates to rhenium followed by the migration of the methyl to the coordinated oxygen atom of Re−OOH has the lowest energy barrier. To determine whether the reaction of **1** with H_2O_2 in the presence of OH^- proceeds via an OMBV pathway to form the alkoxide complex **3**, as the reaction of **1** and IO_4^- does (see above), the reaction of complex **1** with a mixture of 5 equiv of H_2O_2 and 5 equiv of NaOH in 1:1 THF-d_8/D_2O (v/v) was monitored at −1.3 °C by ^{1}H NMR spectroscopy. Under these conditions, the starting material **1** converts to complex **2** in 10 min. Complex **2** then undergoes slow transformation to $TMSCH_2OH$ over a period of 8 h. Consequently, alcohol release from complex **1** and H_2O_2 in the presence of hydroxide proceeds by an η^2-peroxo pathway that involves two steps: the formation of the η^2-peroxo complex **2** and the conversion of **2** to $TMSCH_2OH$. Compared to the reaction with H_2O_2 under acidic conditions, the reaction rates of both steps (i.e., formation of **2** and release of $TMSCH_2OH$) are faster with hydroxide. For example, the reaction of complex **1** with a mixture of H_2O_2 (3 equiv) and HCl (3 equiv) produces complex **2** in hours at room temperature, which then converts to $TMSCH_2OH$ in 48 h (Scheme 8).

Scheme 8. Comparison of Alcohol Release from Cp*W(O)$_2$(CH_2SiMe_3) (1) with H_2O_2 in the Presence of H^+ and OH^-

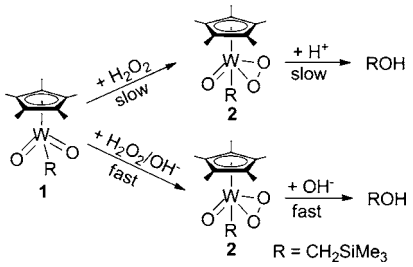

DFT was used to probe the conversion of dioxo complex **1** and hydrogen peroxide to the η^2-peroxo complex **2** (Scheme 9). A [2 + 2] addition of the OH bond of hydrogen peroxide across the W=O bond of **1** (red line in Scheme 9) has a calculated barrier of 28 and 30 kcal·mol^{-1} for 1,4-dioxane and water, respectively. This [2 + 2] TS leads to the hydroxy/hydroperoxy intermediate Cp*W(R)(O)(OH)(OOH), which is 10 kcal·mol^{-1} above complex **1**. From this intermediate, a modest barrier of 12 kcal·mol^{-1} (1,4-dioxane) or 14 kcal·mol^{-1} (water) must be surmounted to transfer hydrogen from the hydroperoxide to hydroxide ligand to dissociate water and yield complex **2**. Overall, with HO_2^-/OH^- as the oxygen atom transfer couple, the transformation of **1** to **2** is calculated to be mildly endergonic by 3 kcal·mol^{-1} in both 1,4-dioxane and water. Deprotonation of hydrogen peroxide and coordination of hydroperoxide gives Cp*W(O)$_2$(R)(OOH), which is higher in energy than **1** by 10 and 13 kcal·mol^{-1}. Conversion of Cp*W(O)$_2$(R)(OOH) to complex **2** through an intramolecular proton transfer and dissociation of hydroxide are calculated to occur with overall activation barriers of 28 and 27 kcal·mol^{-1}. Thus, the calculations do not reveal any obvious advantage to base-promoted conversion of **1** and hydrogen peroxide to complex **2**.

dx.doi.org/10.1021/ja309755g | J. Am. Chem. Soc. 2013, 135, 424−435

Scheme 9. Calculated Free Energy for the Conversion of $Cp^*W(O)_2(CH_2SiMe_3)$ (1) and H_2O_2 to $Cp^*WO(\eta^2\text{-}O)_2(CH_2SiMe_3)$ (2)[a]

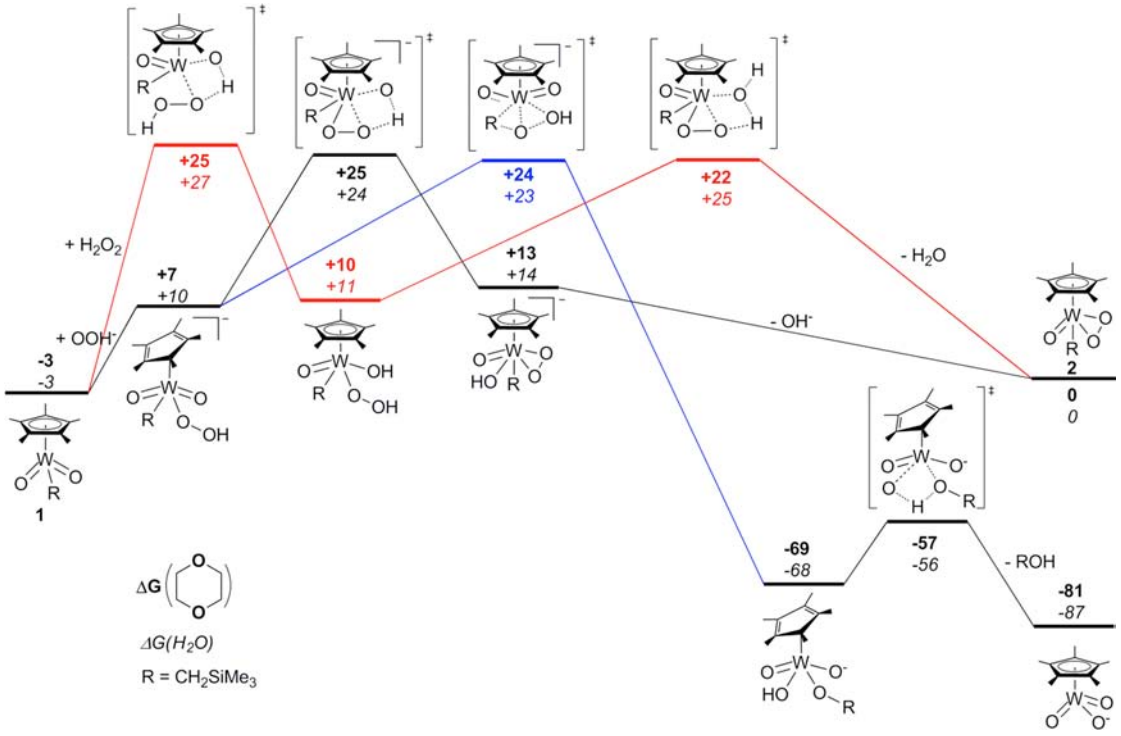

[a]Numbers are free energies (kcal·mol^{-1}) for 1,4-dioxane/water and are relative to complex **2**.

SUMMARY AND CONCLUSIONS

Insertion of oxygen atoms into metal–hydrocarbyl bonds is a potential key step in catalytic oxidation of hydrocarbons. Despite the potential importance of such oxygen atom insertion reactions, there are few examples of nonradical conversion of M–R bonds and oxygen atom transfer reagents to M–OR, and detailed studies of nonradical oxygen atom insertion into M–R bonds are rare. We have established that Cp^*W^{VI} complexes can undergo clean oxygen atom insertion reactions by at least *three different pathways* (Scheme 10). Oxy-insertion from η^2-peroxide complexes can be promoted by addition of hydroxide or Brønsted acid. DFT calculations lead to the suggestion that protonation of the η^2-peroxide ligand facilitates alkyl migration to the unprotonated oxygen atom. Our calculations suggest that the addition of base leads to a similar TS in which the alkyl group migrates to the unprotonated oxygen of an η^2-hydroperoxide ligand; however, the base-promoted TS is overall anionic and has a second oxo ligand (Scheme 11).

Scheme 10. Summary of Pathways for the Oxygen Atom Insertion into W–C Bonds of $Cp^*W(O)_2(CH_2SiMe_3)$ (1) and $Cp^*W(O)(\eta^2\text{-}O)_2(CH_2SiMe_3)$ (2)

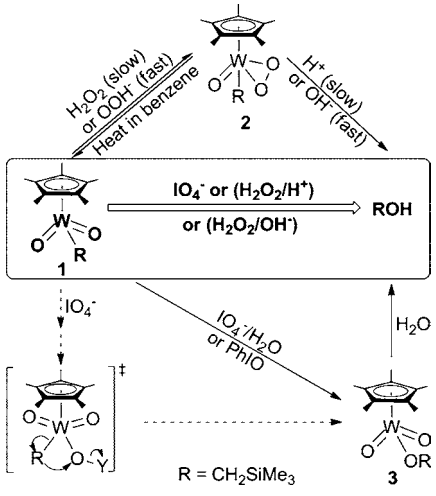

Scheme 11. Comparison of TSs Based on DFT Calculations for Base- and Acid-Promoted Conversion of $Cp^*W(O)(\eta^2\text{-}O)_2(CH_2SiMe_3)$ (2) to the Oxy-Insertion Products

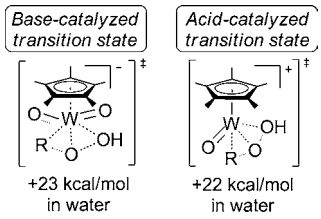

Experiments clearly show that the base-promoted oxy-insertion is faster than the acid-catalyzed reaction. Quantification of such effects is important, since most successful transition-metal-catalyzed alkane oxidations incorporate electrophilic late transition metals that tolerate acidic conditions but are not likely to be amenable to alkaline conditions.[6,45] Some caution is advised when comparing these calculated values, since most computations use an implicit water solvation model and calculations for the reaction of **1** and IO_4^- with explicit water demonstrate that hydrogen bonding can be important. The third oxy-insertion follows an OMBV pathway. To our knowledge, this is only the second example of an oxygen atom

dx.doi.org/10.1021/ja309755g | J. Am. Chem. Soc. 2013, 135, 424–435

insertion into a M−R bond that likely proceeds by this concerted process.[15] Importantly, the OMBV reaction with **1** occurs in neutral water/1,4-dioxane, suggesting that catalysts with nucleophilic hydrocarbyl groups that are tolerant of water should be amenable for this oxy-functionalization process.

EXPERIMENTAL SECTION

General Methods. Unless otherwise noted, all synthetic procedures were performed under anaerobic conditions in a nitrogen-filled glovebox or by using standard Schlenk techniques. Glovebox purity was maintained by periodic nitrogen purges and was monitored by an oxygen analyzer (O_2 < 15 ppm for all reactions). Tetrahydrofuran and 1,4-dioxane were dried by distillation from sodium/benzophenone and P_2O_5, respectively. Diethyl ether was distilled over CaH_2. THF-d_8, 1,4-dioxane-d_8, D_2O, and $H_2{}^{18}O$ were used as received and stored under a N_2 atmosphere over 4 Å molecular sieves (except water). ^{1}H NMR spectra were recorded on a Varian Mercury 300 or Varian Inova 500 MHz spectrometer. All ^{1}H spectra are referenced against residual proton signals of the deuterated solvents. GC/MS was performed using a Shimadzu GCMS-QP2010 Plus system with a 30 mm × 0.25 mm SHRXI-5MS column with 0.25 mm film thickness using negative chemical ionization (NCI), which also allows for simulated electron impact (SEI) ionization. The preparation, isolation, and characterization of Cp*W(O)$_2$(CH_2SiMe_3) and Cp*W(O)(η^2-O_2)(CH_2SiMe_3) have been previously reported.[39] All other reagents were used as purchased from commercial sources.

Computational Methods. DFT calculations with the B3LYP[46−48] functional employed the Gaussian 09 program[49] in conjunction with the pseudopotentials and valence basis sets of Stevens and co-workers[50,51] for W, Si, and I. All 2p elements plus hydrogen were modeled with the 6-311++G(d,p) all-electron basis set. All species were singlet spin states and optimized within the restricted Kohn−Sham formalism with the exception of $\mathbf{1}^{\bullet-}$and $[IO_4]^{\bullet}$, which are doublets and optimized with unrestricted Kohn−Sham methods. For the latter, spin contamination was minimal. All stationary points were optimized in the gas phase without symmetry constraint and identified as minima or TSs through the calculation of the energy Hessian. Solvent effects were incorporated implicitly through the use of the CPCM[52] model for water and 1,4-dioxane. All quoted energetics are free energies and are reported, assuming a temperature of 298.15 K and 1 atm and were obtained using unscaled vibrational frequencies.

Reaction of Cp*W(O)$_2$(CH_2SiMe_3) (1) with $NaIO_4$. Complex **1** (2.1 mg, 5.0 μmol) was dissolved in 300 μL of THF-d_8 in an NMR tube. $NaIO_4$ (3.3 mg, 15 μmol) was dissolved in 300 μL of D_2O and transferred to the solution of **1**. The reaction was monitored by ^{1}H NMR spectroscopy until completion. The production of $TMSCH_2OH$ was confirmed using two methods. First, 5 μL of the reaction mixture was analyzed by GC/MS, and $TMSCH_2OH$ was detected (and compared with GC/MS of an authentic sample). Second, 1 μL of $TMSCH_2OH$ was added to the reaction mixture. The intensity of the product peaks increased in the ^{1}H NMR spectrum. Cp*W(O)$_2$(OCH_2SiMe_3) (**3**): ^{1}H NMR (THF-d_8/D_2O 1:1): 4.17 (CH_2, s), 2.04 (CH_3, s), −0.05 ($Si(CH_3)_3$, s) ppm.

Kinetics of Reactions of Cp*W(O)$_2$(CH_2SiMe_3) (1) with $NaIO_4$. A representative kinetic experiment is described. Complex **1** (32.0 mg 75.0 μmol) was dissolved in 4.5 mL of THF-d_8. Two drops of benzene were added to the solution as an internal standard for ^{1}H NMR integration. A 300 μL aliquot (0.0166 mol/L) was transferred to an NMR tube. $NaIO_4$ (143 mg, 0.667 mmol) was dissolved in 2.0 mL of D_2O (0.33 mol/L). D_2O (225 μL) was added to the solution of **1** by syringe and cooled in ice water. Then, 75 μL (5.0 equiv) of the $NaIO_4$ solution was added to the solution of complex **1**. The reaction mixture was then monitored by array ^{1}H NMR spectroscopy on a 500 MHz spectrometer at −1.3 °C. A ^{1}H NMR spectrum was acquired every 26 s. Integration of the methylene peak of complex **1**, $TMSCH_2OH$, and the intermediate **3** gave the variation in concentrations. Similar reactions were set up for 10.0, 15.0, and 20.0 equiv of $NaIO_4$ by adjusting the amounts of the D_2O and $NaIO_4$ solution. To ensure reproducibility, every concentration was repeated in triplicate.

Eyring Plot of Reaction of Cp*W(O)$_2$(CH_2SiMe_3) (1) with $NaIO_4$. A representative kinetic experiment is described. Complex **1** (13.5 mg, 32.0 μmol) was dissolved in 4.8 mL of THF-d_8. Two drops of benzene were added to the solution as an internal standard for ^{1}H NMR integration. A 300 μL aliquot (0.0067 mol/L) was transferred to an NMR tube by syringe. $NaIO_4$ (44.8 mg, 0.200 mmol) was dissolved in 6.0 mL of D_2O (0.033 mol/L). The solution of complex **1** was cooled in ice water. Then, 300 μL (5.0 equiv) of the $NaIO_4$ solution was added to the solution of complex **1**. The reaction mixture was monitored by array ^{1}H NMR spectroscopy on a 500 MHz spectrometer at 10.7 °C. A ^{1}H NMR spectrum was acquired every 2 min. Integration of the methylene peak of complex **1** gave the variation in concentrations. Similar reactions were set up at −1.3, 22.7, and 34.7 °C. The time between every ^{1}H NMR spectrum in the array was adjusted according to the rate of the reaction. To ensure reproducibility, every concentration was repeated at least twice for a minimum of three total experiments under each set of conditions.

Oxygen Labeling of Reaction of Cp*W(O)$_2$(CH_2SiMe_3) (1) with $NaI^{18}O_4$. $NaIO_4$ (10.7 mg, 50.0 μmol) was dissolved in 300 μL of $H_2{}^{18}O$ and allowed to equilibrate for 1 h at room temperature with sonication (the exchange of ^{18}O and ^{16}O under such condition is extremely fast).[53] Complex **1** (4.2 mg, 10 μmol) was dissolved in 300 μL of THF, and the solution was transferred to the $NaIO_4$ solution. After 20 min at room temperature, the color of the solution faded from pale yellow to colorless. A 3.0 μL aliquot of the reaction mixture was analyzed by GC/MS for $TMSCH_2OH$ content. The fragmentation pattern of $TMSCH_2OH$ produced from the reaction was compared to patterns for $TMSCH_2{}^{18}OH$ and $TMSCH_2{}^{16}OH$.

Reaction of Cp*W(O)$_2$(CH_2SiMe_3) (1) with PhIO. Complex **1** (4.2 mg, 10 μmol) and PhIO (8.0 mg, 30 μmol) was dissolved in 400 μL of 1,4-dioxane-d_8 in a J-Young tube. The tube was then taken out of the box and sonicated for 30 min. ^{1}H NMR spectroscopy was used to monitor the reaction.

Reaction of Cp*W(O)$_2$(CH_2SiMe_3) (1) with $[Bu_4N][IO_4]$. Complex **1** (4.3 mg, 10 μmol) and $[Bu_4N][IO_4]$ (12.9 mg, 30.0 μmol) were dissolved in 300 μL of dry THF-d_8. ^{1}H NMR spectroscopy was used to monitor the reaction at room temperature. No reaction was observed after 24 h. D_2O (300 μL) was added to the reaction mixture. A ^{1}H NMR spectrum was acquired after 2 h, and quantitative formation of $TMSCH_2OH$ was observed.

Kinetics of Water Dependence in the Reaction of Cp*W(O)$_2$(CH_2SiMe_3) (1) with $[Bu_4N][IO_4]$. A representative kinetic experiment is described. Complex **1** (32.0 mg 75.0 μmol) and $[Bu_4N][IO_4]$ (487 mg, 1.12 mmol, 15 equiv) were dissolved in 6.0 mL of THF-d_8. Two drops of benzene were added to the solution as an internal standard for ^{1}H NMR integration. A 400 μL aliquot was transferred to a J-Young tube. D_2O (5.0 μL, 50 equiv) was added to the solution of **1** and $[Bu_4N][IO_4]$ by syringe. The reaction mixture was then monitored by array ^{1}H NMR spectroscopy on a 500 MHz spectrometer at 50 °C. A ^{1}H NMR spectrum was acquired every 20 min. Integration of the methylene peak of complex **1** gave the variation in concentrations. Similar procedures were used to set up the reaction of **1** and 15 equiv of $[Bu_4N][IO_4]$ with 10.0, 20.0, 30.0, 40.0, 60.0, and 100 μL of D_2O (for the reaction with 60.0 and 100 μL of D_2O, the same amount of **1** and $[Bu_4N][IO_4]$ were dissolved in 300 μL of THF-d_8 instead of 400 μL). To ensure reproducibility, every concentration was repeated in triplicate.

Reaction of Cp*W(O)(η^2-O_2)(CH_2SiMe_3) (2) with NaOH. Complex **2** (4.3 mg, 10 μmol) was dissolved in 300 mL of THF-d_8 in an NMR tube. NaOH (1.2 mg, 30 μmol) was dissolved in 300 μL of D_2O and transferred to the solution of complex **1**. The reaction mixture was monitored by ^{1}H NMR spectroscopy until completion. The production of $TMSCH_2OH$ was confirmed using two methods. First, 5 μL of the reaction mixture was analyzed by GC/MS, and $TMSCH_2OH$ was detected (and compared with GC/MS of an authentic sample). Second, 1 μL of $TMSCH_2OH$ was added to the reaction mixture. The intensity of the product peaks increased in ^{1}H NMR spectrum.

Kinetics of Cp*W(O)(η^2-O_2)(CH_2SiMe_3) (2) with NaOH. A representative kinetic experiment is described. Complex **1** (33.0 mg,

dx.doi.org/10.1021/ja309755g | J. Am. Chem. Soc. 2013, 135, 424−435

75.0 μmol) was dissolved in 4.5 mL of THF-d_8. Several milligrams of hexamethylbenzene were added to the solution as an internal standard for ^{1}H NMR integration. A 300 μL aliquot (0.0166 mol/L) was transferred to an NMR tube. NaOH (26.7 mg, 0.667 mmol) was dissolved in 2.0 mL of D_2O (0.33 mol/L). D_2O (225 μL) was added to the solution of complex **1** by syringe and cooled in ice water. Then, 75 μL (5.0 equiv) of the NaOH solution was added to the complex **1** solution. The reaction mixture was then monitored by array ^{1}H NMR spectroscopy on a 500 MHz spectrometer at 10.7 °C. A ^{1}H NMR spectrum was acquired every 2 min. Integration of the Cp* methyl peak of complex **2** and the methylene peak of $TMSCH_2OH$ gave the variation in concentrations. Similar reactions were set up for 10.0, 15.0, and 20.0 equiv of NaOH by adjusting the amounts of the D_2O and NaOH solutions. The time between every ^{1}H NMR spectrum in the array was adjusted according to the rate of the reactions. To ensure reproducibility, every concentration was repeated in triplicate.

Eyring Plot of Reaction of Cp*W(O)(η^2-O_2)(CH_2SiMe_3) (2) with NaOH. A representative kinetic experiment is described. Complex **2** (35.2 mg, 80.4 μmol) was dissolved in 4.8 mL of THF-d_8. Several milligrams of hexamethylbenzene were added to the solution as an internal standard for ^{1}H NMR integration. A 300 μL aliquot (0.0166 mol/L) was transferred to an NMR tube by syringe. NaOH (20.2 mg, 0.505 mmol) was dissolved in 6.0 mL of D_2O (0.083 mol/L). The solution of complex **1** was cooled in ice water. Then, 300 μL (5.0 equiv) of the NaOH solution was added to the solution of complex **1**. The reaction mixture was then monitored by array ^{1}H NMR spectroscopy on a 500 MHz spectrometer at 10.7 °C. A ^{1}H NMR spectrum was acquired every 2 min. Integration of the Cp* methyl peak of complex **2** and the methylene peak of $TMSCH_2OH$ gave the variation in concentrations. Similar reactions were set up at −1.3, 22.7, and 34.7 °C. The time between every ^{1}H NMR spectrum in the array was adjusted according to the rate of the reaction. To ensure reproducibility, every concentration was repeated in triplicate.

Oxygen Labeling of Reaction of Cp*W(O)(η^2-O_2)(CH_2SiMe_3) (2) with Li*OH. $H_2{}^{18}O$ (300 μL) was transferred to a vial and frozen in an ^{i}PrOH/dry ice bath. CH_3Li in diethyl ether solution (1 M, 30 μL) was added to the frozen $H_2{}^{18}O$. The *i*PrOH/dry ice bath was then removed, and the mixture was warmed up to room temperature to generate the $Li^{18}OH$ in $H_2{}^{18}O$ solution. Complex **2** (4.3 mg, 10 μmol) was dissolved in 300 μL of THF, and the solution was added to the $Li^{18}OH$ solution. After 30 min at room temperature, a 3.0 μL aliquot of the reaction mixture was analyzed by GC/MS for $TMSCH_2OH$ content. The fragmentation pattern of $TMSCH_2OH$ from the reaction was compared to patterns for $TMSCH_2{}^{18}OH$ and $TMSCH_2{}^{16}OH$.

Reaction of Cp*W(O)(η^2-O_2)(CH_2SiMe_3) (2) with Brønsted Acid. A representative reaction is described. Complex **2** (2.2 mg, 5.0 μmol) was dissolved in 400 μL of 1,4-dioxane-d_8 in a J-Young tube, and HCl in diethyl ether solution (1N, 15 μL) was added to the solution of **2**. The reaction was then monitored by ^{1}H NMR spectroscopy. The reaction was complete after approximately 2 days.

Reaction of Cp*W(O)$_2$(CH_2SiMe_3) (1) with H_2O_2/H^+. Complex **1** (4.2 mg, 10 μmol) was dissolved in 300 μL of 1,4-dioxane-d_8 in an NMR tube. Hydrochloric acid (35%, 3.0 μL, 33 μmol) and H_2O_2 (30%, 3.0 μL, 29 μmol) were added to 300 μL of D_2O. The mixture of H_2O_2 and HCl was then added to the complex **2** solution. ^{1}H NMR spectroscopy was used to monitor the reaction at room temperature.

Reaction of Cp*W(O)$_2$(CH_2SiMe_3) (1) with H_2O_2/OH^-. Complex **1** (4.2 mg, 10 μmol) was dissolved in 300 μL of 1,4-dioxane-d_8 in an NMR tube. NaOH (1.2 mg, 30 μmol) was dissolved in 300 μL of D_2O, and H_2O_2 (30%, 3.0 μL, 29 μmol) was added to the NaOH solution. The mixture of H_2O_2 and NaOH was then added to the solution of **2**. ^{1}H NMR spectroscopy was used to monitor this reaction at room temperature.

Kinetics of Reaction of Cp*W(O)$_2$(CH_2SiMe_3) (1) with H_2O_2/OH^-. Complex **1** (4.2 mg, 10 μmol) was dissolved in 300 μL of THF-d_8 in an NMR tube. NaOH (2.0 mg, 50 μmol) was dissolved in 300 μL of D_2O and 5 μL (48 μmol) of 30% H_2O_2 solution was added to the NaOH solution. Both starting materials were cooled in ice water. The mixture of H_2O_2 and NaOH was then added to the solution of **2**. The reaction mixture was then monitored by array ^{1}H NMR spectroscopy on a 500 MHz spectrometer at −1.3 °C. A ^{1}H NMR spectrum was acquired every 26 s.

Kinetics of Reaction of Cp*W(O)$_2$(CH_2SiMe_3) (1) and Cp*W(O)(η^2-O_2)(CH_2SiMe_3) (2) with H_2O_2/OH^-. A mixture of complex **1** (2.1 mg, 5.0 μmol) and complex **2** (2.2 mg, 5.0 μmol) was dissolved in 300 μL of THF-d_8 in an NMR tube. NaOH (2.0 mg, 50 μmol) was dissolved in 300 μL of D_2O, and 5 μL (48 μmol) of a 30% H_2O_2 solution was added to the NaOH solution. Both starting materials were cooled in ice water. The mixture of H_2O_2 and NaOH was then added to the solution of **2**. The reaction mixture was then monitored by array ^{1}H NMR spectroscopy on a 500 MHz spectrometer at −1.3 °C. A ^{1}H NMR spectrum was acquired every 26 s.

■ ASSOCIATED CONTENT

Supporting Information

Kinetics and GC/MS data, additional experimental details, and computational details. This material is available free of charge via the Internet at http://pubs.acs.org.

■ AUTHOR INFORMATION

Corresponding Author

tbg7h@virginia.edu; t@unt.edu

Notes

The authors declare no competing financial interest.

■ ACKNOWLEDGMENTS

This work was solely supported as part of the Center for Catalytic Hydrocarbon Functionalization, an Energy Frontier Research Center funded by the U.S. Department of Energy, Office of Science, Office of Basic Energy Sciences, under award no. DE-SC0001298.

■ REFERENCES

(1) Olah, G. A.; Molnár, A. *Hydrocarbon Chemistry*, 2nd ed.; John Wiley & Sons: Hoboken, NJ, 2003.

(2) Wittcoff, H. A.; Reuben, B. G.; Plotkin, J. S. *Industrial Organic Chemicals*, 2nd ed.; John Wiley & Sons: Hoboken, NJ, 2004.

(3) Conley, B. L.; Tenn, W. J.; Young, K. J. H.; Ganesh, S.; Meier, S.; Ziatdinov, V.; Mironov, O.; Oxgaard, J.; Gonzales, J.; Goddard, W. A.; Periana, R. A. Methane Functionalization. In *Activation of Small Molecules*; Tolman, W. B., Ed.; Wiley-VCH: Weinheim, Germany, 2006; Chapter 7, p 235.

(4) Crabtree, R. H. *J. Chem. Soc., Dalton Trans.* **2001**, 2437.

(5) Labinger, J. A.; Bercaw, J. E. *Nature* **2002**, *417*, 507.

(6) Labinger, J. A. *J. Mol. Catal. A: Chem.* **2004**, *220*, 27.

(7) Periana, R. A.; Bhalla, G.; Tenn Iii, W. J.; Young, K. J. H.; Liu, X. Y.; Mironov, O.; Jones, C. J.; Ziatdinov, V. R. *J. Mol. Catal. A: Chem.* **2004**, *220*, 7.

(8) *Activation and Functionalization of C-H Bonds*; Goldberg, K. I., Goldman, A. S., Eds.; ACS Symposium Series 864; American Chemical Society: Washington, DC, 2004.

(9) Conley, B. L.; Tenn Iii, W. J.; Young, K. J. H.; Ganesh, S. K.; Meier, S. K.; Ziatdinov, V. R.; Mironov, O.; Oxgaard, J.; Gonzales, J.; Goddard Iii, W. A.; Periana, R. A. *J. Mol. Catal. A: Chem.* **2006**, *251*, 8.

(10) Webb, J. R.; Bolaño, T.; Gunnoe, T. B. *ChemSusChem* **2011**, *4*, 37.

(11) Chepaikin, E. G. *Usp. Khim.* **2011**, *80*, 363.

(12) Shilov, A. E.; Shul'pin, G. B. *Chem. Rev.* **1997**, *97*, 2879.

(13) Stahl, S. S.; Labinger, J. A.; Bercaw, J. E. *Angew. Chem., Int. Ed.* **1998**, *37*, 2180.

(14) Lersch, M.; Tilset, M. *Chem. Rev.* **2005**, *105*, 2471.

(15) Conley, B. L.; Ganesh, S. K.; Gonzales, J. M.; Tenn, W. J.; Young, K. J. H.; Oxgaard, J.; Goddard, W. A.; Periana, R. A. *J. Am. Chem. Soc.* **2006**, *128*, 9018.

(16) Tenn, W. J.; Young, K. J. H.; Bhalla, G.; Oxgaard, J.; Goddard, W. A.; Periana, R. A. *J. Am. Chem. Soc.* **2005**, *127*, 14172.

(17) Feng, Y.; Lail, M.; Barakat, K. A.; Cundari, T. R.; Gunnoe, T. B.; Petersen, J. L. *J. Am. Chem. Soc.* **2005**, *127*, 14174.
(18) Figg, T. M.; Webb, J. R.; Cundari, T. R.; Gunnoe, T. B. *J. Am. Chem. Soc.* **2011**, *134*, 2332.
(19) Conner, D.; Jayaprakash, K. N.; Wells, M. B.; Manzer, S.; Gunnoe, T. B.; Boyle, P. D. *Inorg. Chem.* **2003**, *42*, 4759.
(20) Wang, S. H.; Mandimutsira, B. S.; Todd, R.; Ramdhanie, B.; Fox, J. P.; Goldberg, D. P. *J. Am. Chem. Soc.* **2003**, *126*, 18.
(21) Conner, D.; Jayaprakash, K. N.; Wells, M. B.; Manzer, S.; Gunnoe, T. B.; Boyle, P. D. *Inorg. Chem.* **2003**, *42*, 4759.
(22) Feng, Y.; Lail, M.; Foley, N. A.; Gunnoe, T. B.; Barakat, K. A.; Cundari, T. R.; Petersen, J. L. *J. Am. Chem. Soc.* **2006**, *128*, 7982.
(23) Hashiguchi, B. G.; Young, K. J. H.; Yousufuddin, M.; Goddard, W. A.; Periana, R. A. *J. Am. Chem. Soc.* **2010**, *132*, 12542.
(24) Kloek, S. M.; Heinekey, D. M.; Goldberg, K. I. *Angew. Chem., Int. Ed.* **2007**, *46*, 4736.
(25) Bercaw, J. E.; Hazari, N.; Labinger, J. A. *Organometallics* **2009**, *28*, 5489.
(26) Van Asselt, A.; Trimmer, M. S.; Henling, L. M.; Bercaw, J. E. *J. Am. Chem. Soc.* **1988**, *110*, 8254.
(27) Matsunaga, P. T.; Hillhouse, G. L.; Rheingold, A. L. *J. Am. Chem. Soc.* **1993**, *115*, 2075.
(28) Alsters, P. L.; Boersma, J.; van Koten, G. *Organometallics* **1993**, *12*, 1629.
(29) Brown, S. N.; Mayer, J. M. *J. Am. Chem. Soc.* **1994**, *116*, 2219.
(30) Koo, K.; Hillhouse, G. L.; Rheingold, A. L. *Organometallics* **1995**, *14*, 456.
(31) Brown, S. N.; Mayer, J. M. *J. Am. Chem. Soc.* **1996**, *118*, 12119.
(32) Blackburn, T. F.; Labinger, J. A.; Schwartz, J. *Tetrahedron Lett.* **1975**, *16*, 3041.
(33) Brindley, P. B.; Scotton, M. J. *J. Chem. Soc., Perkin Trans.* **1981**, *2*, 419.
(34) Kamaraj, K.; Bandyopadhyay, D. *Organometallics* **1999**, *18*, 438.
(35) Vaughan, G. A.; Rupert, P. B.; Hillhouse, G. L. *J. Am. Chem. Soc.* **1987**, *109*, 5538.
(36) Abu-Omar, M. M.; Hansen, P. J.; Espenson, J. H. *J. Am. Chem. Soc.* **1996**, *118*, 4966.
(37) Gonzales, J. M.; Distasio, R.; Periana, R. A.; Goddard, W. A.; Oxgaard, J. *J. Am. Chem. Soc.* **2007**, *129*, 15794.
(38) Bischof, S. M.; Cheng, M.-J.; Nielsen, R. J.; Gunnoe, T. B.; Goddard, W. A.; Periana, R. A. *Organometallics* **2011**, *30*, 2079.
(39) Legzdins, P.; Phillips, E. C.; Sanchez, L. *Organometallics* **1989**, *8*, 940.
(40) Kim, G. S.; Huffman, D.; DeKock, C. W. *Inorg. Chem.* **1989**, *28*, 1279.
(41) Chisholm, M. H.; Folting, K.; Huffman, J. C.; Kirkpatrick, C. C. *Inorg. Chem.* **1984**, *23*, 1021.
(42) Richardson, D. E. *Kinetica98*; Department of Chemistry, University of Florida: Gainesville, FL, 1998.
(43) Kassim, A. Y.; Sulfab, Y. *Inorg. Chem.* **1981**, *20*, 506.
(44) Wang, W.-D.; Espenson, J. H. *J. Am. Chem. Soc.* **1998**, *120*, 11335.
(45) Hashiguchi, B. G.; Bischof, S. M.; Konnick, M. M.; Periana, R. A. *Acc. Chem. Res.* **2012**, *45*, 885.
(46) Lee, C.; Yang, W.; Parr, R. G. *Phys. Rev. B* **1988**, *37*, 785.
(47) Becke, A. D. *J. Chem. Phys.* **1993**, *98*, 5648.
(48) Becke, A. D. *J. Chem. Phys.* **1993**, *98*, 1372.
(49) Frisch, M. J.; Trucks, G. W.; Schlegel, H. B.; Scuseria, G. E.; Robb, M. A.; Cheeseman, J. R.; Scalmani, G.; Barone, V.; Mennucci, B.; Petersson, G. A.; Nakatsuji, H.; Caricato, M.; Li, X.; Hratchian, H. P.; Izmaylov, A. F.; Bloino, J.; Zheng, G.; Sonnenberg, J. L.; Hada, M.; Ehara, M.; Toyota, K.; Fukuda, R.; Hasegawa, J.; Ishida, M.; Nakajima, T.; Honda, Y.; Kitao, O.; Nakai, H.; Vreven., T.; Montgomery, Jr., J. A. ; Peralta, J. E.; Ogliaro, F.; Bearpark, M.; Heyd, J. J.; Brothers, E.; Kudin, K. N.; Staroverov, V. N.; Kobayashi, R.; Normand, J.; Raghavachari, K.; Rendell, A.; Burant, J. C.; Iyengar, S. S.; Tomasi, J.; Cossi, M.; Rega, N.; Millam, J. M.; Klene, M.; Knox, J. E.; Cross, J. B.; Bakken, V.; Adamo, C.; Jaramillo, J.; Gomperts, R.; Stratmann, R. E.; Yazyev, O.; Austin, A. J.; Cammi, R.; Pomelli, C.; Ochterski, J. W.; Martin, R. L.; Morokuma, K.; Zakrzewski, V. G.; Voth, G. A.; Salvador, P.; Dannenberg, J. J.; Dapprich, S.; Daniels, A. D.; Farkas, O.; Foresman, J. B.; Ortiz, J. V.; Cioslowski, J.; Fox, D. J. *Gaussian*, Revision B.01; Gaussian Inc: Wallingford, CT, 2009.
(50) Stevens, W. J.; Basch, H.; Krauss, M. *J. Chem. Phys.* **1984**, *81*, 6026.
(51) Stevens, W. J.; Krauss, M.; Basch, H.; Jasien, P. G. *Can. J. Chem.* **1992**, *70*, 612.
(52) Cossi, M.; Rega, N.; Scalmani, G.; Barone, V. *J. Comput. Chem.* **2003**, *24*, 669.
(53) Pecht, I.; Luz, Z. *J. Am. Chem. Soc.* **1965**, *87*, 4068.